

PartSTAD: 2D-to-3D Part Segmentation Task Adaptation

Hyunjin Kim
KAIST

rlaguswls98@kaist.ac.kr

Minhyuk Sung
KAIST

mhsung@kaist.ac.kr

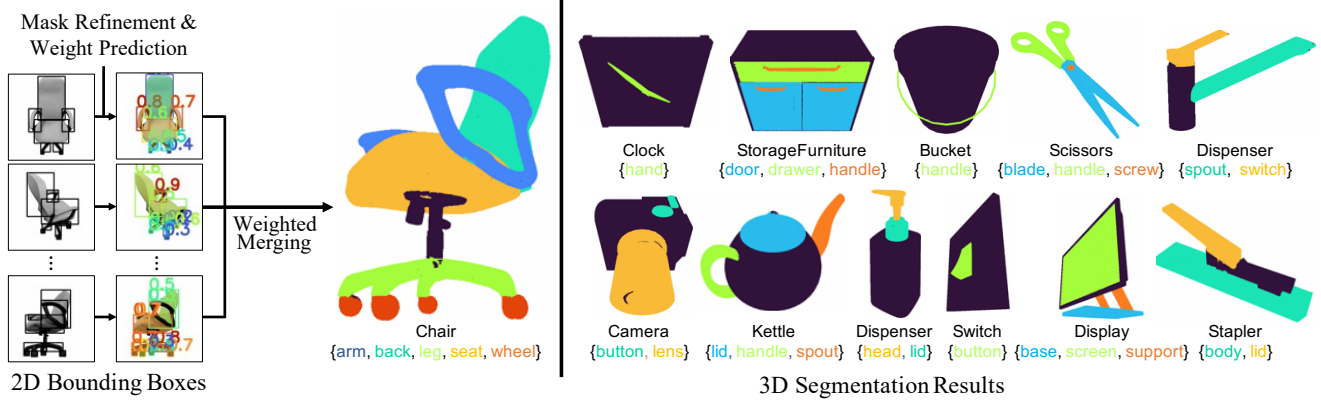


Figure 1. We introduce PARTSTAD, a novel few-shot 3D point cloud part segmentation method that leverages 2D-to-3D task adaptation. By obtaining 2D segmentation masks in multi-view images from GLIP [25] and SAM [20] and optimizing the mask weights for 3D segmentation as a learning objective, it can successfully predict fine-grained parts with accurate boundaries, as shown in the figure above.

Abstract

We introduce PARTSTAD, a method designed for the task adaptation of 2D-to-3D segmentation lifting. Recent studies have highlighted the advantages of utilizing 2D segmentation models to achieve high-quality 3D segmentation through few-shot adaptation. However, previous approaches have focused on adapting 2D segmentation models for domain shift to rendered images and synthetic text descriptions, rather than optimizing the model specifically for 3D segmentation. Our proposed task adaptation method finetunes a 2D bounding box prediction model with an objective function for 3D segmentation. We introduce weights for 2D bounding boxes for adaptive merging and learn the weights using a small additional neural network. Additionally, we incorporate SAM, a foreground segmentation model on a bounding box, to improve the boundaries of 2D segments and consequently those of 3D segmentation. Our experiments on the PartNet-Mobility dataset show significant improvements with our task adaptation approach, achieving a **7.0%p** increase in mIoU and a **5.2%p** improvement in mAP₅₀ for semantic and instance segmentation compared to the SotA few-shot 3D segmentation model.

1. Introduction

3D segmentation has been a subject of extensive research in computer vision due to its central role in various downstream applications involving the understanding of shape structure, functionality, mobility, and semantics. However, the limited availability of annotated 3D shapes has remained a bottleneck in achieving generalizability in learned segmentation models for diverse 3D data. Annotating 3D segmentation is particularly labor-intensive, time-consuming, and requires expertise in handling 3D models. For this reason, the scale of 3D part-level annotations remains in the tens of thousands [37], while the scale of 2D annotation datasets in the image domain, for example, exceeds a million [20, 30].

Recent research [2, 32] has illuminated the potential of visual-language models bridging textual descriptions with images in accomplishing zero-shot or few-shot 3D segmentation results. The basic idea is to render a 3D model from various viewpoints, conduct 2D detection or segmentation on the rendered images, and then aggregate the 2D segmentation results into a 3D representation using either a voting mechanism [32] or a label propagation scheme [2]. This approach is not only effective in enabling zero-shot and few-shot 3D segmentation but also offers an advantage in that

the set of part names does not need to be predefined in training but can be determined at test time.

PartSLIP [32] is a notable example that achieves 3D part segmentation results comparable to fully supervised methods while adapting a pretrained 2D detection model with few-shot training for 3D segmentation. It leverages the pretrained GLIP [25] model for 2D detection, associating the output 2D bounding boxes with one of the tokens (part names) provided in the input prompt. Its key component is the GLIP finetuning process, which introduces a small number of learnable parameters to the frozen GLIP model and trains them using few-shot synthetic images and texts employed in the 3D segmentation pipeline. As GLIP was initially trained with real photos and natural language descriptions of objects by humans, this adaptation to rendered images and the unconventional description (a sequence of part names) results in a substantial improvement in the 3D segmentation task.

Despite promising initiatives, it is important to note that the previous approach was limited to achieving *domain adaptation*. In contrast, we emphasize that in the 2D-to-3D segmentation lifting task, not only does the data domain change, but the task itself also shifts from 2D segmentation to 3D segmentation. Thus, the process of applying the pretrained model to the new task requires *task adaptation*, involving modifying the model with an objective function associated with the new task. Particularly for 3D segmentation, it is necessary to integrate 2D segmentation results from multiple viewpoints into a coherent 3D representation. Therefore, it is crucial to control the noise of 2D bounding box predictions in the context of its impact on the final 3D segmentation after integration.

Specifically, our Part Segmentation Task ADaptation method, PARTSTAD, adapts the pretrained GLIP model with a relaxed 3D mIoU loss while incorporating bounding boxes across all different views. Instead of typical finetuning, we draw inspiration from recent work [16, 32] that introduces small learnable parameters to the existing model while keeping existing parameters frozen. As a result, we train a small MLP using 2D bounding box features extracted from the pretrained GLIP model. Since the relaxed mIoU loss is non-differentiable with respect to the bounding box positions, we suggest predicting a *weight* for each bounding box instead of adjusting its position. This results in minimal modification in the 2D-to-3D voting scheme while achieving a significant improvement in 3D segmentation, even with few-shot training, e.g., with eight objects per category, as done in PartSLIP. To further enhance 3D segmentation performance, we leverage SAM [20], a 2D instance segmentation model, to segment the foreground region within each bounding box, obtaining an accurate boundary for each 2D segment.

In our experiments on the PartNet-Mobility [55] dataset,

we showcase the superior performance of our method in comparison to recent zero-shot/few-shot 3D semantic and instance segmentation methods that leverage 2D segmentation models. In contrast to the SotA few-shot method, our approach achieves a **7.0%p** improvement in semantic segmentation mIoU and a **5.2%p** improvement in instance segmentation mAP₅₀. These improvements are consistent across all object classes.

2. Related Work

2.1. Supervised 3D Segmentation

Given the availability of open segment-annotated 3D datasets [3, 5, 7, 8, 12, 14, 37, 55], 3D segmentation has been extensively researched in the last several years, focusing on the development of novel network architectures for supervised learning. Regarding the architecture of semantic segmentation, diverse models have been explored, including PointNet [42] and its variants [36, 43, 44, 56, 70], those using CNN [27, 34, 49, 58], GCN [17, 28, 53], and Transformers [54, 59, 66, 72]. For instance segmentation, various approaches based on proposing 3D bounding boxes [15, 60, 65], clustering learned features [11, 19, 31, 38, 50, 51, 68, 73], and combining both semantic and instance segmentations [29, 40, 46, 52] have been introduced. Despite these great advances, the performance of supervised methods has been limited by the scale of 3D datasets; the largest part-annotated 3D dataset, PartNet [37], includes fewer than 30k models.

There have been some attempts to overcome the limitation by leveraging additional weak supervisions, such as text descriptions of objects [21], 3D bounding box annotations [10], sparse labels [26, 35], and geometric priors [23, 24]. However, the scale of this additional data has also been limited to tens of thousands, while datasets in the image domain are on the scale of millions.

2.2. 3D Segmentation Using Vision-Language Models

Recent work introduced ideas about exploiting vision-language models (VLM) for 3D segmentation. The advantage of utilizing the learned visual-language grounding in 3D segmentation lies in the strong generalizability to arbitrary 3D models with zero-shot or few-shot training, and also in the open vocabulary understanding that enables labeling points without specifying the set of part or object names during training. For a VLM, CLIP [45] has been adapted in multiple previous works to lift the 2D grounding to the 3D, detecting parts in an object [13] and objects in a scene [9, 39, 47, 69], while the results are limited to highlighting some regions without providing clear segment boundaries.

To obtain precise segments in 3D, other 2D object

detection and segmentation models, such as SAM [20], GLIP [25], and GroundingDINO [33], are also leveraged. SAM3D [62] was an example of directly lifting the 2D masks from SAM to 3D with a bottom-up merging approach, although it was limited to segmenting the parts, not labeling them. SA3D [6] utilized NeRF representation and allowed user interaction for 3D segmentation, but it can be inefficient when the 3D objects are given as a mesh, point cloud, or other common 3D representations. OpenMask3D [47] and OpenIns3D [18] are concurrent works, both of which combine multiple foundation models, SAM [20] and CLIP [45] for OpenMask3D, and GroundingDINO [33] and LISA [22] for OpenIns3D. These works focus on segmenting objects in 3D scenes, while we aim to do finer-grained segmentation, finding parts in 3D objects.

PartSLIP [32] and SATR [2] are notable examples that achieve part segmentation of 3D objects based on a 2D object detection model, GLIP [25]. They obtain 2D bounding boxes on the rendered images from multiple views and integrate them over the 3D object with different merging schemes. The finetuning of GLIP introduced by PartSLIP particularly leads to a performance improvement, but it is limited to domain adaptation, not task adaptation. Building on this, we introduce a novel task adaptation technique as well as integration with SAM [20] to achieve a further significant improvement in 3D segmentation accuracy.

2.3. Task Adaptation

Taskonomy [67] is a seminal work that introduced the concept of task transfer learning for the first time, enabling the transformation of an image dense prediction model trained for a base task to perform other tasks through finetuning. Pruksachatkun *et al.* [41] also introduced a similar idea for language-domain tasks. Later, task adaptation has been extensively studied to leverage features learned from generative models, such as GAN [71] and diffusion models [4, 48, 57, 61], adapting them with a small network for various tasks, including image segmentation [4, 57, 71], depth prediction [48], and keypoint detection [61]. For 3D tasks, Abdelreheem *et al.* [1] are notable examples of using vision language-grounding models for 3D correspondence but are limited to directly applying 2D priors without finetuning. We introduce a novel task adaptation technique that lifts 2D segments to 3D by adapting the 2D features during the training of a small network with a task-specific objective function.

3. Background and Preliminaries

Recent research [2, 13, 32] has demonstrated how vision-language models designed for image object detection and segmentation can be applied to segment parts in 3D objects. The main idea involves rendering a 3D model from various viewpoints, performing 2D detection or segmentation for

the rendered image at each view, and then combining the 2D segmentation results over the 3D model.

Specifically, SATR [2] utilizes GLIP [25] as the 2D detection model. To obtain 2D bounding boxes for each of the specified part names, it feeds a concatenated list of these part names (separated by commas) as the input prompt to the pretrained GLIP model, along with a rendered image. The 2D bounding boxes are then mapped to a single face of the input 3D mesh, located at the center of the respective 2D bounding box, and the part names are propagated throughout the entire mesh based on geodesic distances. Similarly, PartSLIP [32] also leverages GLIP [25] for 2D detection but employs a different voting scheme for the 2D bounding box integration over the 3D object, which utilizes the over-segmentation of the input point cloud. One key distinction between PartSLIP and SATR is that PartSLIP proposes to modify the GLIP model for domain adaptation to the rendered images and text prompts used in 3D segmentation. Specifically, the text prompt is given as a concatenation of part names in the PartSLIP pipeline, which is not a typical and natural description of the object. Therefore, it learns a category-specific constant offset vector for the language embedding feature in the given pairs of prompts and rendered images, while keeping the GLIP parameters frozen.

Our work builds upon the PartSLIP pipeline. In the following subsections, we describe the details of its major components: the voting scheme, and the finetuning process.

3.1. PartSLIP [32]

The main technical components of PartSLIP are the 1) voting scheme based on super points and 2) adaptation to text prompts¹. We describe the details of each component below.

Voting for Super Points PartSLIP first over-segments the input 3D object represented as a point cloud \mathcal{P} into a set of super points $P_i \subseteq \mathcal{P}$, which provide geometric priors for the boundaries of the parts. The 3D object is rendered into K viewpoints, and the 2D bounding boxes for each image are predicted using GLIP [25]. Let \mathcal{B} denote the entire set of 2D bounding boxes from all views, and $B_{jk} \subseteq \mathcal{B}$ indicates a subset that includes the bounding boxes classified as the j -th part label from the k -th view. $V_k : \mathcal{P} \rightarrow \{0, 1\}$ is a function indicating whether the input point is visible from the k -th viewpoint. Also, for each 2D bounding box $b \in \mathcal{B}$, $I_b : \mathcal{P} \rightarrow \{0, 1\}$ is a function indicating whether the input point is included in the bounding box b . Given these, the voting aggregating the semantic labels of the 2D bounding boxes to the 3D point cloud is performed by calculating the following score s_{ij} for each pair of the i -th super point and

¹Although multi-view feature aggregation is also introduced, the improvement by this component is marginal, and the author of PartSLIP also did not include this component in their official code. Therefore, we will omit this part in our review.

the j -th label:

$$s_{ij} = \frac{\sum_k \sum_{p \in P_i} V_k(p) (\max_{b \in (B_{jk} \cup \{b_\emptyset\})} I_b(p))}{\sum_k \sum_{p \in P_i} V_k(p)}, \quad (1)$$

where b_\emptyset is a *null* bounding box, and we assume that I_{b_\emptyset} for the null bounding box returns zero for any input point (simplifying notations for the case when $B_{jk} = \emptyset$). Note that this $s_{ij} \in [0, 1]$ denotes the ratio of visible points from each view included in any of the 2D bounding boxes labeled with the j -th label. Finally, for each i -th super point, the label with the highest score s_{ij} across all the labels is assigned to the super point. Exceptionally, if the highest score is less than a null label threshold s_\emptyset , which is set to 0.5 in our experiments, the null label is assigned to the super point.

GLIP Finetuning While GLIP demonstrates impressive generalizability for unseen images and prompts, it still has limitations when it comes to handling synthetic images and text prompts, such as the rendered images and sequences of part names used in the PartSLIP pipeline. To address this, the authors of PartSLIP propose adding small, learnable parameters to the GLIP model while keeping all the pretrained GLIP parameters frozen. These new parameters are learned with very few-shot examples: 8 annotated 3D objects per category. They represent offset feature vectors for each part name and remain constant as global variables for each category, rather than changing for each input. This adaptation of GLIP significantly improves the accuracy of 3D part segmentation.

Instance Segmentation The voting scheme described above is designed for semantic segmentation, but PartSLIP also introduces a straightforward merging-based method to achieve instance segmentation based on semantic segmentation. To obtain instance segments, it merges adjacent super points under two conditions: 1) they share the same semantic label, and 2) they are either both included or both excluded for all bounding boxes.

4. PARTSTAD: Task Adaptation for 2D-to-3D

PartSLIP has demonstrated that adapting a 2D detection model for 3D segmentation with a small set of trainable parameters can significantly enhance 3D segmentation performance. However, we observe that PartSLIP’s adaptation is limited to *domain adaptation*, where it learns new parameters using synthetic images and data used in the PartSLIP framework without altering the *objective function* during training.

When applying the 2D segmentation model to 3D segmentation, it is important to note that not only does the data domain change, but the *task* itself changes. Therefore, through the process of incorporating 2D bounding boxes

into the 3D object, the 2D bounding box prediction model must align with our ultimate goal: 3D part segmentation.

To address this, we introduce Part Segmentation Task ADaptation method, PARTSTAD, a *task adaptation* approach designed to finetune the 2D segmentation model for 3D part segmentation. In Sec. 4.1, we introduce our objective function to finetune the GLIP for the 3D segmentation task. In Sec. 4.2, we describe how we adapt the pretrained GLIP model with the new objective function by introducing additional learnable parameters and modifying the voting scheme (Eq. 1). PartSLIP also faces a performance limitation due to the GLIP that provides 2D bounding boxes, not 2D segments. In Sec. 4.3, we also propose to combine the SAM[20] foreground mask for each bounding box to obtain more precise 2D segments and, consequently, further improve the 3D segmentation.

4.1. 3D mRIoU Loss

We begin by describing the loss function that we use for adapting the GLIP to the 3D segmentation task. Let \mathbf{l}_j and $\hat{\mathbf{l}}_j \in \{0, 1\}^{|\mathcal{P}|}$ be binary vectors indicating whether each point p in \mathcal{P} has the j -th label in the ground truth and label prediction, respectively. The mean Intersection over Union (mIoU) for the predicted 3D segmentation, the standard evaluation metric for 3D segmentation, is defined as follows:

$$\text{mIoU}(\{\mathbf{l}_j\}, \{\hat{\mathbf{l}}_j\}) = \frac{1}{M} \sum_{j=1}^M \frac{\mathbf{l}_j^\top \hat{\mathbf{l}}_j}{\|\mathbf{l}_j\|_1 + \|\hat{\mathbf{l}}_j\|_1 - \mathbf{l}_j^\top \hat{\mathbf{l}}_j}, \quad (2)$$

where M is the number of labels.

Our goal is to use the 3D mIoU as the objective function directly when adapting the GLIP model. However, the mIoU is non-differentiable. Thus, we employ a relaxed version known as mean Relaxed IoU (mRIoU) [24, 64], which simply allows the predicted indicator vectors $\hat{\mathbf{l}}_j$ to be non-binary: $\hat{\mathbf{l}}_j \in [0, 1]^{|\mathcal{P}|}$. The loss $\mathcal{L}_{\text{mRIoU}}$ is specifically defined as follows:

$$\mathcal{L}_{\text{mRIoU}} = 1 - \text{mIoU}(\{\mathbf{l}_j\}, \{\hat{\mathbf{l}}_j\}). \quad (3)$$

In the appendix, we demonstrate that the choice of the loss function, as compared to other alternatives such as the cross-entropy loss, is crucial to achieving a substantial improvement in our task adaptation.

Note that in the PartSLIP framework, where super points are utilized in 3D segmentation, and $s_{ij} \in [0, 1]$ indicates the likelihood of the i -th super point belonging to the j -label, the mRIoU can be calculated by defining \mathbf{l}_j based on $\mathbf{s}_j = [s_{1j}, s_{2j}, \dots]^\top$ as follows:

$$\hat{\mathbf{l}}_j = \mathbf{M} \mathbf{s}_j, \quad (4)$$

where $\mathbf{M} \in \{0, 1\}^{|\mathcal{P}| \times |\{P_i\}|}$ is a binary matrix that describes the memberships from each point to the super points.

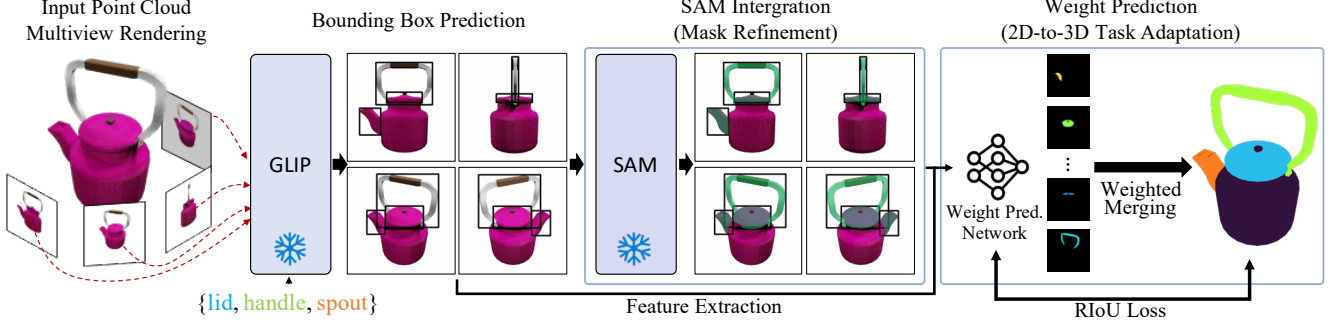


Figure 2. **Overall pipeline of PARTSTAD.** Our approach begins by rendering the provided 3D point cloud from multiple viewpoints. Subsequently, we extract 2D bounding boxes for its parts using GLIP [25] (Bounding Box Prediction); note that we utilize the finetuned GLIP model from PartSLIP [32]. Following this, we convert the bounding boxes into segmentation masks using SAM [20], extracting the foreground region for each bounding box (SAM Mask Integration). Next, we predict weights for all the masks and adaptively combine them into a 3D representation (2D-to-3D task adaptation). The final step involves obtaining the segmentation label for the input point cloud. The GLIP and SAM models are frozen, while only our novel weight prediction network is trained per category in a few-shot setting (8 objects).

4.2. Bounding Box Weight Prediction

A typical approach for adapting a pretrained model to a new task would be finetuning the model using an objective function tailored to that new task. However, the finetuning method generally fails to yield meaningful improvements, especially when the goal is to achieve few-shot adaptation (e.g., with only 8 annotated 3D objects per class, as done in our case), while the pretrained model has been trained on an extensive dataset. To address this challenge, recent works like LoRA [16] and PartSLIP [32] have introduced the concept of adding small learnable parameters while keeping the existing pretrained model parameters frozen. This approach not only makes training very efficient but also enables the model to generalize effectively to unseen data.

While we also follow this approach, our specific challenge arises from the fact that when we use the 3D mRIoU (Eq. 3) as the objective function for 3D segmentation, it becomes non-differentiable with respect to the 2D bounding box location, which is the output of GLIP. This non-differentiability arises from the computation of the score s_{ij} (Eq. 1) for each pair of super point and label.

To address this, we propose training a small network that does not refine the location but instead predicts a *weight* for each 2D bounding box, taking the learned features of the boxes as input. If we denote the output weight of the network for bounding box b as $W(b) \in \mathbb{R}^+$, the score s_{ij} for a pair of super point and label is modified to \tilde{s}_{ij} as follows:

$$\tilde{s}_{ij} = \frac{\sum_k \sum_{p \in P_i} V_k(p) (\max_{b \in (B_{jk} \cup \{b_\emptyset\})} I_b(p) W(b))}{\sum_k \sum_{p \in P_i} V_k(p)}. \quad (5)$$

Note that the change is simply to multiply the weight $W(b)$ by $I_b(p)$, while only $I_b(p)$, indicating whether the point p is included in bounding box b , has been used in Eq. 1. This

modified score no longer falls within the range of $[0, 1]$. The final score \bar{s}_{ij} is thus defined by normalizing \tilde{s}_{ij} using the softmax function over the set of labels:

$$\bar{s}_{ij} = \frac{\exp(\tilde{s}_{ij})}{\sum_j \exp(\tilde{s}_{ij})}. \quad (6)$$

We additionally propose to make the unnormalized score for the null label \tilde{s}_\emptyset *learnable* in our case, initialized with 10. We thus compute the softmax above while including \tilde{s}_\emptyset . The label of each super point is still chosen as the label giving the highest score \bar{s}_{ij} , becoming null if the normalized null label score \bar{s}_\emptyset becomes the highest.

Network Architecture We design the weight predictor network to take the bounding box feature vectors \mathbf{f}_b from the pretrained GLIP model as input. The feature vectors of all bounding boxes across all views are fed to the network at once and processed with a small shared two-layer MLP. Context normalization [63] is added in the middle of the two layers to incorporate contextual information from the global set of boxes for each box. The output of the MLP for each bounding box is further processed with the following modified ReLU function $\phi(\cdot)$:

$$\phi(\mathbf{x}) = \max(\tau + \mathbf{x}, 0), \quad (7)$$

where τ is a user-defined constant offset (10 in our experiments).

4.3. SAM [20] Mask Integration

Another limitation of PartSLIP is its reliance on GLIP [25] for 2D segmentation. Since GLIP is, in turn, a 2D object detection model, it produces bounding boxes instead of 2D segments, which cannot provide accurate boundaries of segments. We propose to address this issue by incorporating another pretrained 2D segmentation model, SAM [20].

SAM has the functionality of taking a bounding box as input and producing the foreground mask. Using this, we replace the set of 2D bounding boxes \mathcal{B} with a set of 2D masks, while preserving the remaining steps in the framework. Note that the point-to-bounding-box membership I_b is changed to point-to-mask membership, and we still use the same bounding box features extracted from GLIP corresponding to each mask to train the weight prediction network. We demonstrate the effectiveness of applying the SAM mask in our experiments in Sec. 5.

5. Experiment Results

In the experiments, we compare our method with the SotA 2D-prior-based zero-shot/few-shot 3D segmentation models using the PartNet-Mobility [55] dataset. In the **appendix**, we present additional results on the ablation study, outcomes with scanned data, and comprehensive results covering all PartNet-Mobility categories.

5.1. Experiment Setup

Dataset We use the PartNet-Mobility [55] dataset, which is also used in the experiments of PartSLIP [32]. The PartNet-Mobility [55] dataset includes 45 object categories. For each category, the training split includes 8 shapes, while the test split has a range of the number of objects from 6 to 338, totaling 1,906 objects across all 45 categories. Following PartSLIP, 8 shapes from the test set of each category are designated as the validation set. To obtain the 2D bounding boxes for each object, we use 10 images from fixed viewpoints across all our experiments.

Evaluation Metrics As evaluation metrics, we employ the *mean Intersection over Union (mIoU)* metric for semantic segmentation and *mean Average Precision (mAP)* for instance segmentation.

For semantic segmentation, the average mIoU over the entire dataset is computed by first calculating it per semantic part, averaging them across the parts in the same category, resulting in category-level mIoU, and then averaging the category-level mIoUs again across all the categories.

For instance segmentation, we compute two types of mAP: *part-aware* mAP and *part-agnostic* mAP. For part-aware mAP, similar to mIoU in semantic segmentation, we first calculate the mAP for each semantic part with instances having the part label. We then average them for each category, and then across categories. For part-agnostic mAP, we do not consider the semantic labels and directly compute the category-level mAP with part instances in the same object category, and then average them. All mAP values correspond to mAP_{50} with an IoU threshold of 50%.

Baselines We compare our method with three baselines: PartSLIP [32], SATR [2], and SAM3D [62].

- **PartSLIP** [32] is the method that we adopt as our base. Note that PartSLIP uses a finetuned GLIP model, and we also employ the same model in our framework to extract bounding box features for our task adaptation.
- **SATR** [2] is similar to PartSLIP, conducting 3D segmentation using 2D bounding boxes from GLIP [25]. However, SATR differs from PartSLIP in four key aspects: 1) it does not involve finetuning the GLIP model, 2) it does not utilize super points, 3) it is designed for mesh segmentation, not point cloud segmentation, and 4) it employs a distinct approach for integrating 2D bounding boxes into 3D (label propagation). To ensure a fair comparison between our method and SATR, we implement the following changes to SATR. First, since we employ the GLIP model finetuned by PartSLIP in our framework, we use the same finetuned model within the SATR framework. Second, we convert the point cloud input to a mesh, performing mesh segmentation with SATR, and apply the results to the input point cloud by finding the closest vertex for each point. Lastly, we introduce a version of SATR using super points, resulting in a comparison between our method and two versions of SATR: one without super points (denoted as *SATR*) and one with super points (denoted as *SATR+SP*). Since SATR does not perform instance segmentation, our comparison with it is focused on semantic segmentation.
- **SAM3D** [62] is another zero-shot 3D segmentation method using a 2D segmentation model, not GLIP [25], but SAM [20]. Since it only performs instance segmentation but does not label each segment, we compare our method with it only for instance segmentation, using the part-agnostic mAP metric.

Ablation Study We also conduct an ablation study, comparing our method with two major components being ablated: the weight prediction (Sec. 4.2) and the SAM mask integration (Sec. 4.3). In the **appendix**, we also compare our method with cases using cross-entropy loss instead of mRIoU loss (Sec. 4.1) and using GLIP bounding box confidence score instead of our learned weights in the weighted voting (Sec. 4.2).

5.2. Semantic Segmentation Results

Tab. 1 and Fig. 3 present the quantitative and qualitative comparisons of part semantic segmentation results, respectively. Please refer to the appendix for the complete table encompassing all 45 categories. In comparison to PartSLIP [32], a SotA few-shot 3D segmentation method, we achieve a significant **7.0%p mIoU** improvement over the entire set of 45 categories. Furthermore, for each specific category, we consistently demonstrate improvement, sur-

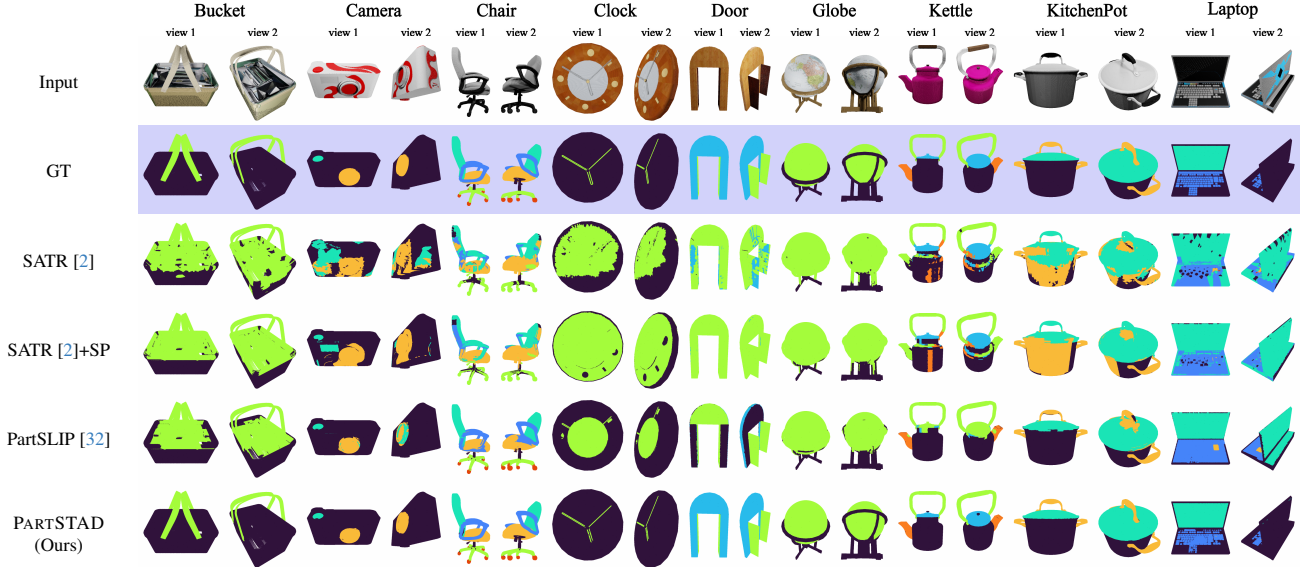


Figure 3. Qualitative comparison of semantic segmentation results. Our PARTSTAD segments 3D parts more precisely with clearer boundaries, even for small (Camera, Chair) and thin (Clock) parts.

Method	Mean	Storage Furniture	Table	Faucet	Chair	Switch	Trash Can	Toilet	Eye-glasses	Globe	Cart	Window	Bottle	Dispenser	Laptop	Coffee Machine	USB	Remote	Pen	Dish-washer	Scissors
SATR [2]	29.3	20.6	23.3	37.1	33.1	21.4	11.6	17.6	63.5	83.1	30.8	67.7	50.0	38.2	11.2	20.0	30.2	17.2	51.1	12.9	36.8
SATR [2]+SP	34.8	28.9	28.0	39.8	37.7	37.0	15.9	22.1	74.2	83.5	37.2	69.2	55.5	41.4	12.4	23.2	33.4	28.0	57.3	18.8	43.0
PartSLIP [32]	58.0	52.3	44.6	66.2	82.8	52.1	23.3	50.4	89.2	92.9	78.7	78.3	80.7	70.8	31.2	37.2	52.1	36.6	68.9	59.1	61.4

Ablation Study																					
w/o Weight Pred.	61.9	56.6	45.0	65.5	85.0	51.9	24.3	56.6	88.7	98.1	85.4	72.6	85.9	70.5	31.5	36.6	57.1	36.6	64.3	61.4	60.8
w/o SAM Integration	62.1	54.0	45.7	64.0	83.1	53.0	18.4	49.4	92.1	95.7	81.2	78.6	81.0	72.0	33.6	37.1	53.6	46.8	65.1	59.2	67.5
PARTSTAD (Ours)	65.0	59.5	47.8	65.3	85.3	57.9	21.2	57.5	92.5	93.5	85.0	76.1	83.6	73.7	34.6	35.8	59.9	53.4	60.6	60.5	68.5

Table 1. Quantitative comparison of the semantic segmentation results (mIoU(%)) on the PartNet-Mobility dataset. Ours achieves a **7.0%p** improvement in average mIoU compared to PartSLIP [32], the SotA few-shot 3D segmentation method, while consistently increasing mIoU across all categories. Please refer to the appendix for the complete table with results for all 45 categories.

passing by more than 15%p in some categories (e.g., Remote). Qualitatively, the results also highlight the effectiveness of our task adaptation and the SAM mask integration in segmenting parts more precisely, even for small (e.g., Camera, Chair) and thin (e.g., Clock) parts of objects.

SATR exhibits inferior performance, even when leveraging the finetuned GLIP model and super points (see SATR+SP results) due to the label-propagation-based 2D bounding box integration, which often fails to provide clear boundaries in 3D segmentation, as illustrated in Fig. 3.

The ablation study results demonstrate the influence of each major component in our framework. The quantitative findings indicate that the weight prediction network plays a crucial role in substantial improvement, leading to a 3.1%p decrease in average mIoU when it is ablated. The SAM mask integration also contributes significantly, resulting in a 2.9%p average mIoU decrease when ablated.

5.3. Instance Segmentation Results

Following the instance segmentation idea of PartSLIP, we also perform instance segmentation using our method and compare the quantitative results with those of other methods in Tab. 2 and Tab. 3, reporting part-aware mAPs and part-agnostic mAPs, respectively. Fig. 4 also displays qualitative comparisons across different methods. Please refer to the appendix for the complete table of all 45 categories. Similar to semantic segmentation, ours achieves **4.0%p** and **5.2%p** improvements for both average part-aware mAPs and part-agnostic mAPs, respectively. Both the weight prediction network and SAM mask integration also exhibit meaningful improvements in performance, as their influence is depicted in the ablation study results. Compared to SAM3D [62], whose part-agnostic mAPs are shown in Tab. 3, our method achieves much better performance with more than three times greater mAP. Qualitative results also illustrate the outstanding performance of our method, accu-

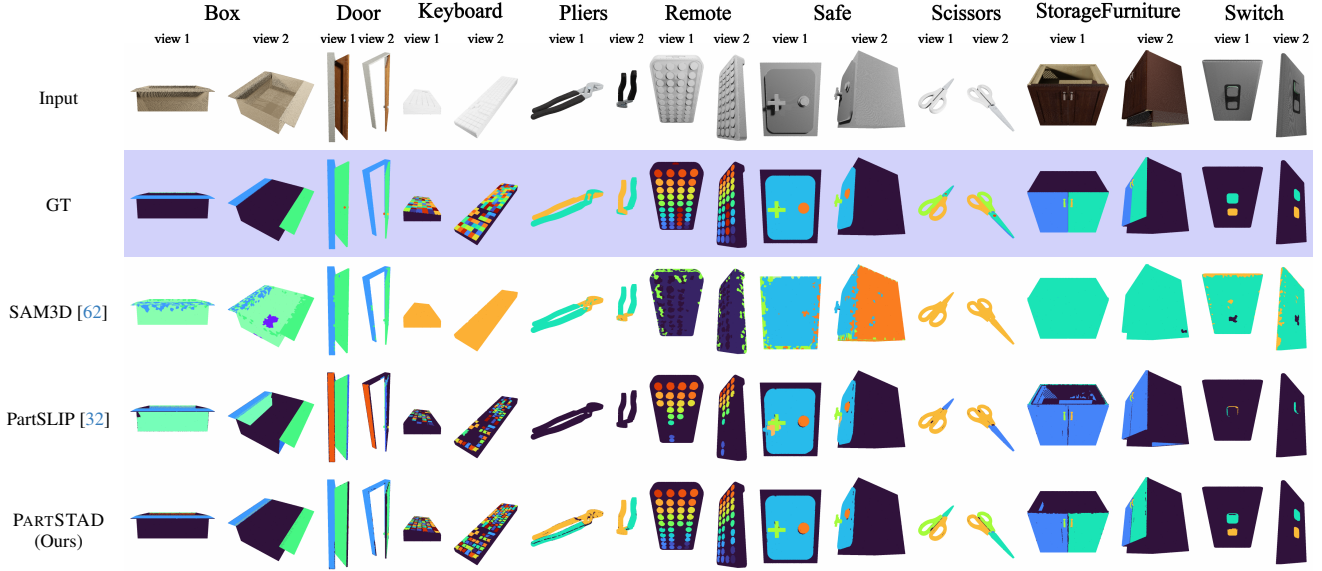


Figure 4. Qualitative comparison of instance segmentation results shows that our PARTSTAD successfully segments tiny 3D parts, such as the keys of keyboards and buttons of remote controls, with clear segment boundaries.

Method	Mean	Storage Furniture	Table	Faucet	Chair	Trash Can	Switch	Toilet	Eye-glasses	Globe	Cart	Window	Dispenser	Bottle	Laptop	Coffee Machine	USB	Remote	Pen	Dish-washer	Scissors
PartSLIP [32]	41.6	29.1	32.6	43.0	82.2	11.6	21.2	36.2	69.8	92.1	69.5	23.6	56.3	73.4	17.8	15.8	20.9	19.9	49.5	40.3	23.6
Ablation Study																					
<i>w/o Weight Pred.</i>	44.7	33.8	30.8	39.9	82.5	12.2	22.2	40.8	68.5	100.0	74.0	19.3	60.7	74.9	24.4	15.5	17.4	20.3	39.4	41.7	25.5
<i>w/o SAM Integration</i>	44.2	29.4	32.3	38.5	82.2	12.7	19.7	36.0	70.3	98.8	68.3	26.1	67.4	79.5	23.6	15.5	24.8	29.6	53.5	44.7	23.1
PARTSTAD(Ours)	45.6	35.5	33.2	35.3	82.5	11.6	22.1	40.6	72.0	84.3	71.6	19.9	65.5	77.4	28.9	13.8	26.5	33.7	39.0	50.3	26.5

Table 2. Part-aware mAPs(%) of the instance segmentation results on the PartNet-Mobility dataset. Ours achieves **4.0%p** improvement in mean part-aware mAPs compared to PartSLIP [32], with consistent enhancements across all categories. Please refer to the appendix for the complete table with results for all 45 categories.

Method	Mean	Storage Furniture	Table	Faucet	Chair	Trash Can	Switch	Toilet	Eye-glasses	Globe	Cart	Window	Dispenser	Bottle	Laptop	Coffee Machine	USB	Remote	Pen	Dish-washer	Scissors
SAM3D [62]	12.1	1.2	10.6	24.0	5.5	9.6	5.4	3.7	27.6	3.9	8.6	18.0	20.7	16.0	1.5	3.6	22.6	1.0	8.0	6.7	7.2
PartSLIP [32]	38.9	29.7	28.7	42.8	80.7	22.6	21.2	35.4	71.8	92.1	69.5	23.6	59.0	73.4	19.5	9.8	20.5	19.9	40.8	39.0	27.0
Ablation Study																					
<i>w/o Weight Pred.</i>	42.6	35.9	29.2	37.1	81.1	24.5	22.2	40.0	72.1	100.0	74.0	19.3	59.9	74.9	26.5	9.5	15.2	20.3	35.8	41.9	29.4
<i>w/o SAM Integration</i>	42.6	34.8	27.6	37.9	81.2	24.4	19.7	36.6	72.5	98.8	68.3	26.1	69.0	79.5	27.4	9.4	27.3	29.6	47.2	47.1	24.9
PARTSTAD (Ours)	44.1	41.7	28.2	35.6	83.3	22.8	22.4	41.0	74.0	84.3	71.2	19.5	65.5	76.2	34.1	9.4	23.5	33.7	34.5	49.7	26.2

Table 3. Part-agnostic mAPs(%) of the instance segmentation results on the PartNet-Mobility dataset. Ours demonstrates **5.2%p** improvement in mean part-agnostic mAPs compared to PartSLIP [32], surpassing SAM3D with a mean mAP that is more than three times larger. Please refer to the appendix for the complete table with results for all 45 categories.

rately identifying all the tiny instances of parts, such as keys on keyboards, buttons on remotes, and clear boundaries of these instances.

6. Conclusion

We presented PARTSTAD, a task adaptation method for lifting 2D segmentation to 3D. Instead of directly finetuning a 2D segmentation network, our method learns a small

neural network predicting weights for each 2D bounding box with an objective function for 3D segmentation, and then performs 3D segmentation via weighted merging of the boxes in 3D. We further improve the performance of 3D segmentation by integrating SAM foreground masks for each bounding box. We achieve the SotA results in few-shot 3D part segmentation, demonstrating significant improvements in both semantic and instance segmentations.

Appendix

In the appendix, we present additional results on the ablation studies (Sec. A.1 and Sec. A.2), outcomes with scanned data (Sec. A.3), and comprehensive results covering all PartNet-Mobility categories (Sec. A.4, Sec. A.5, and Sec. A.6).

A.1. Cross-Entropy Loss vs. mIoU Loss

Method	mIoU (%)
PartSLIP [32] + SAM Mask Integration (Baseline)	61.9
PARTSTAD + Cross-Entropy - mIoU	63.5
PARTSTAD + Cross-Entropy	64.5
PARTSTAD (Ours)	65.0

Table A1. Comparison with the cases of using cross-entropy loss and mIoU loss (Ours).

As mentioned in Sec. 4.1 of the main paper, the use of mIoU loss is crucial for achieving significant improvement in our task adaptation. To demonstrate the effectiveness of our mIoU loss, we conduct an experiment comparing it with the alternative, cross-entropy loss.

Tab. A1 shows the ablation results for different loss types. Baseline at the 1st row in Tab. A1 represents the result which only applies SAM [20] *mask integration* to PartSLIP [32] (same as our method *without weight prediction*). When using the commonly used cross-entropy loss for segmentation tasks, the mIoU decreases by 1.5%p compared to using the mIoU loss. Even when both losses are used together, the mIoU decreases by 0.5%p. This indicates that the mIoU loss is more effective for 3D segmentation task adaptation, and it shows its highest effectiveness when used alone.

A.2. GLIP Confidence Score vs. Mask Weight

Method	mIoU (%)
PartSLIP [32] + SAM Mask Integration (Baseline)	61.9
PARTSTAD + GLIP Conf.	53.3
PARTSTAD + Normalized GLIP Conf.	62.3
PARTSTAD (Ours)	65.0

Table A2. Comparison with the cases of using GLIP confidence score as weight and predicted mask weight (Ours).

It is worth noting that the GLIP [25] model also outputs a confidence score for each predicted bounding box. This implies that we can consider using the GLIP confidence scores as weights in the voting scheme ($W(b)$ in Eq. 5 of the main paper). Thus, we compare the results when us-

ing GLIP confidence scores and the predicted mask weights from our method.

Tab. A2 presents the comparison results between using GLIP confidence as weights and using weights predicted from the network. We compare those methods with the baseline (1st row in Tab. A2) which only applies SAM [20] *mask integration* to PartSLIP [32] (same as our method *without weight prediction*). As the confidence scores from GLIP range in $[0, 1]$, utilizing them directly as weights causes an overall score reduction, resulting in segments are not generated. Consequently, the outcome is notably poor, with a 53.3 mIoU. To ensure a fair comparison, we normalize the weights to maintain the same sum as before. With these normalized weights, as presented in the second row of Tab. A2, the result becomes 62.3 mIoU, a slight increase of 0.4%p compared to the baseline. However, this is still 2.7%p lower than utilizing predicted mask weights from a network trained with 3D mIoU loss. In conclusion, our method provides results more optimized for 3D segmentation than GLIP confidence scores, demonstrating the effectiveness of our method.

As shown in Fig A1, GLIP confidence scores occasionally assign the highest score to incorrect bounding boxes, leading to suboptimal segmentation results. In contrast, the weights predicted by our method consistently assign the highest weight to the correct regions. For instance, using the GLIP confidence score as the weight results in the highest score masks for Bottle (1st row) and Stapler (2nd row) including incorrect regions, leading to inaccuracies in segmentation (indicated by red arrows). In contrast, our method assigns the highest score to the correct mask, indicating that the incorrect mask has a lower score. Additionally, with the GLIP confidence score, the highest score masks for the 3rd and the 4th rows each indicate completely wrong parts (the backside of StorageFurniture). However, our method assigns the highest score to the handle and the correct door part at the front side for the 3rd row and the 4th row, respectively. Those results demonstrate that utilizing the mask weight predicted from the network trained with 3D mIoU loss produces more accurate predictions compared to using the GLIP confidence score as the weight.

A.3. Results on Real-World Scanned Data

Fig. A2 illustrates the results of semantic segmentation on the real-world scan data used in PartSLIP [32]. As seen in the figure, our method demonstrates good results even in real-world scans. Also, our method provides more accurate segmentation than PartSLIP [32]. In the case of the Chair, our method accurately segments the arm part, while PartSLIP fails to do so. For the Kettle, our method better identifies the spout compared to PartSLIP. Additionally, in the cases of StorageFurniture and TrashCan, PartSLIP segments parts that should not be segmented (the backside of

Input		GT		GLIP Confidence				Mask Weight (Ours)			
view 1	view 2	view 1	view 2	Top 1 (view 1)	Seg. Result	view 1	view 2	Top 1 (view 2)	Seg. Result	view 1	view 2

Figure A1. Comparison of results using GLIP confidence scores and Mask Weights. The 5th and the 8th columns depict masks with the highest scores (weights), where red rectangles represent bounding boxes from GLIP, and the white regions are segmentation masks after integrating SAM. From the top row to the bottom, each corresponds to the Bottle, Stapler, and two StorageFurniture categories. When using GLIP confidence, the highest score mask for Bottle (1st row) and Stapler (2nd row) includes an incorrect region, leading to inaccurate segmentation (denoted as red arrows). In contrast, our method assigns the highest score to the correct mask, indicating that the incorrect mask has a lower score. Additionally, when using the GLIP confidence score, the highest score mask for the 3rd and the 4th rows each indicates a completely wrong part (the backside of StorageFurniture). However, our method assigns the highest score to the handle and the correct door part at the front side for the 3rd row and the 4th row, respectively.

StorageFurniture and the lid of TrashCan). On the other hand, for the KitchenPot, while PartSLIP finds the lid part that our method misses, its boundary is still not perfect. We demonstrate that our approach identifies more accurate parts while simultaneously predicting more precise boundaries.

A.4. Complete Quantitative Results of PART-STAD

Tab. A3, Tab. A4, and Tab. A5 show the full table of quantitative results for semantic segmentation, part-aware instance segmentation, and part-agnostic instance segmentation, respectively. Overall, our method demonstrates the best results across whole categories and parts. Please refer to the complete table on the subsequent page for comprehensive information. Moreover, after quantitative result tables, additional qualitative results are illustrated in Sec. A.5 and Sec. A.6.

Category Text Prompt	Cart wheel	Chair arm,back,leg,seat,wheel	Dispenser head,lid	Display base,screen,support	Faucet spout,switch
Input					
PartSLIP [32]					
PARTSTAD (Ours)					

Category Text Prompt	Kettle lid,handle,spout	KitchenPot lid,handle	StorageFurniture door,drawer,handle	Suitcase handle,wheel	TrashCan footpedal,lid,door
Input					
PartSLIP [32]					
PARTSTAD (Ours)					

Figure A2. Qualitative results on real-world scan data. In the highlighted red circle, it is evident that our method achieves more accurate segmentation than PartSLIP [32].

		Baselines			Ablations		
Category	Part	SATR [2]	SATR [2]+SP	PartSLIP [32]	w/o Weight Pred.	w/o SAM Integration	Ours
Bottle	lid	50.0	55.5	80.7	85.9	81.0	83.6
Box	lid	50.6	54.9	77.9	84.3	82.8	81.1
Bucket	handle	6.6	7.5	21.1	85.4	52.4	83.6
Camera	button lens	10.2	20.8	46.1	48.0	53.3	51.6
		24.1	27.5	79.1	77.8	76.6	77.1
Cart	wheel	30.8	37.2	78.8	85.4	81.2	85.0
Chair	arm	22.1	24.4	65.4	68.8	63.5	69.7
	back	52.3	59.4	88.8	88.0	88.2	87.5
	leg	39.8	45.2	90.8	93.1	92.1	93.9
	seat	39.1	46.6	78.8	83.1	78.4	82.7
	wheel	12.1	12.8	90.5	91.9	93.4	92.8
Clock	hand	3.9	16.1	40.5	54.3	46.2	47.4
Coffee Machine	button	2.9	3.6	5.9	5.9	5.8	6.3
	container	41.5	44.9	54.3	52.0	50.6	44.8
	knob	5.6	9.9	28.8	29.0	30.6	31.4
	lid	30.2	34.7	59.9	59.4	61.6	60.7
Dishwasher	door	21.3	20.7	68.6	70.3	67.2	68.1
	handle	4.6	16.9	49.5	52.4	51.3	53.0
Dispenser	head	34.5	36.3	55.2	56.6	59.1	63.2
	lid	42.0	46.4	86.4	84.4	84.9	84.2
Display	base	26.8	33.9	96.7	97.0	95.4	96.8
	screen	35.4	40.0	70.3	73.1	76.3	70.7
	support	19.4	28.0	78.6	80.8	72.1	79.4
Door	frame	14.3	15.1	19.5	20.0	58.4	61.0
	door	55.2	61.4	68.7	72.4	68.9	74.4
	handle	5.9	15.3	47.3	48.2	47.4	48.9
Eyeglasses	body	69.9	78.5	88.2	86.8	95.9	95.8
	leg	57.1	69.8	90.2	90.6	88.3	89.1
Faucet	spout	43.4	46.2	75.3	75.2	74.0	75.3
	switch	30.9	33.4	57.1	55.7	54.1	55.3
Folding Chair	seat	58.1	63.7	83.6	90.4	90.4	91.6
Globe	sphere	83.1	83.5	93.0	98.1	95.7	93.5
Kettle	lid	48.3	55.1	71.8	83.9	89.4	84.1
	handle	17.2	17.5	70.2	89.3	81.3	89.4
	spout	11.3	10.3	78.7	82.6	73.1	79.2
Keyboard	cord	6.3	9.0	89.1	99.0	87.0	91.0
	key	39.4	42.4	55.9	50.6	72.2	73.8
Kitchen Pot	lid	50.1	54.7	76.7	87.0	74.4	72.5
	handle	13.6	14.5	56.9	70.1	64.7	74.5
Knife	blade	36.3	39.9	62.6	64.0	64.4	63.8
Lamp	base	64.9	72.9	88.1	89.3	82.8	89.3
	body	41.5	45.1	77.7	79.6	75.2	82.1
	bulb	0.0	0.0	13.1	13.3	13.0	12.7
	shade	51.9	55.2	86.6	89.4	83.8	89.4
Laptop	keyboard	19.3	24.2	68.3	68.9	68.3	67.9
	screen	18.2	20.7	55.6	58.3	68.5	74.4
	shaft	0.2	0.1	2.7	3.1	3.9	3.4
	touchpad	17.0	14.1	16.2	15.3	14.9	15.5
	camera	1.3	3.1	13.1	11.6	12.2	11.6
Lighter	lid	32.4	32.5	69.8	72.3	67.8	70.9
	wheel	2.0	3.8	51.5	63.0	53.0	64.1
	button	1.6	2.2	58.3	64.3	63.8	62.6

		Baselines			Ablations		
Category	Part	SATR [2]	SATR [2]+SP	PartSLIP [32]	w/o Weight Pred.	w/o SAM Integration	Ours
Microwave	display	1.5	0.0	28.4	28.3	27.9	51.0
	door	17.7	16.6	41.8	52.2	62.2	58.8
	handle	4.5	25.4	77.2	86.9	90.0	84.9
	button	0.7	0.5	23.6	25.7	25.0	41.5
Mouse	button	7.7	6.7	16.7	21.0	8.5	8.8
	cord	29.1	31.0	63.5	65.9	66.2	65.9
	wheel	29.4	64.1	50.9	52.4	45.8	71.9
Oven	door	22.7	22.0	73.6	72.2	78.9	73.4
	knob	2.6	6.1	67.2	67.5	69.3	70.3
Pen	cap	61.4	60.9	68.6	59.3	60.4	50.7
	button	40.8	53.7	69.1	69.2	69.9	70.5
Phone	lid	60.5	63.4	80.0	86.8	80.7	89.8
	button	15.8	20.4	29.6	28.6	34.9	36.5
Pliers	leg	70.2	75.1	46.7	35.5	99.3	99.3
Printer	button	1.2	4.0	5.9	6.3	6.8	7.9
Refrigerator	door	23.2	23.1	57.0	56.4	52.2	52.6
	handle	8.6	24.4	49.7	53.4	40.8	54.5
Remote	button	17.2	28.0	36.5	36.6	46.8	53.4
Safe	door	21.2	24.5	68.0	74.0	62.9	66.5
	switch	3.4	17.0	33.8	35.7	33.4	39.2
	button	6.0	8.2	4.9	5.5	1.2	4.7
Scissors	blade	39.7	47.6	73.3	72.7	75.5	76.1
	handle	59.5	66.5	86.7	87.1	87.8	88.4
	screw	11.2	15.1	23.7	22.7	39.2	40.9
Stapler	body	74.1	87.3	85.7	86.6	84.6	86.0
	lid	65.2	78.5	68.8	76.7	75.2	85.6
Storage Furniture	door	31.6	36.6	50.4	55.1	61.0	63.9
	drawer	25.6	35.5	35.7	37.0	30.5	36.7
	handle	4.7	14.5	71.0	77.7	70.5	77.9
Suitcase	handle	30.3	43.3	77.0	87.4	81.5	82.3
	wheel	20.6	24.2	51.1	52.7	52.3	54.2
Switch	switch	21.4	37.0	52.1	51.9	53.0	57.9
Table	door	0.0	0.0	0.0	0.0	0.0	0.0
	drawer	20.0	25.3	36.7	37.2	38.8	41.8
	leg	42.9	48.6	70.9	72.2	70.3	72.6
	tabletop	46.8	54.4	71.8	79.3	78.6	82.0
	wheel	26.5	30.9	68.0	61.3	63.9	63.7
	handle	3.8	8.7	19.9	20.1	22.6	26.4
Toaster	button	6.4	21.3	51.3	52.0	52.0	52.4
	slider	7.3	17.8	48.6	50.8	66.2	64.8
Toilet	lid	36.6	40.9	69.6	75.9	69.5	77.9
	seat	8.8	11.1	22.6	31.6	16.4	28.6
	button	7.5	14.5	59.1	62.3	62.3	65.9
TrashCan	footpedal	0.0	0.0	0.0	0.0	0.1	0.3
	lid	34.1	47.7	62.0	66.2	54.6	54.6
	door	0.8	0.1	8.0	6.8	0.4	8.7
USB	cap	26.1	27.8	55.1	55.6	52.0	49.9
	rotation	34.4	39.0	49.1	58.6	55.2	69.8
Washing Machine	door	13.4	18.1	57.3	56.7	63.6	56.4
	button	1.3	2.6	32.1	32.7	39.0	39.9
Window	window	67.7	69.2	78.3	72.6	78.6	76.1
Mean		29.3	34.8	58.0	61.9	62.1	65.0

Table A3. Full table of semantic segmentation results on the PartNet-Mobility [55] dataset.

		Baselines	Ablations					Baselines	Ablations		
Category	Part	PartSLIP [32]	w/o Weight Pred.	w/o SAM Integration	Ours	Category	Part	PartSLIP [32]	w/o Weight Pred.	w/o SAM Integration	Ours
Bottle	lid	73.4	74.9	79.5	77.4	Microwave	display	33.7	33.7	33.7	38.1
Box	lid	56.3	72.2	60.7	62.9		door	39.0	23.2	42.7	27.2
Bucket	handle	10.2	78.2	39.3	78.2		handle	50.5	50.5	60.4	50.5
Camera	button	37.6	36.7	39.7	38.7		button	12.0	12.0	12.9	13.6
	lens	35.8	32.7	29.6	29.8	Mouse	cord	5.0	3.0	5.0	5.0
Cart	wheel	69.5	74.0	68.3	71.6		wheel	66.3	66.3	66.3	66.3
								50.5	50.5	50.5	50.5
Chair	arm	59.1	50.2	58.9	50.2	Oven	door	27.9	38.1	32.0	42.5
	back	94.2	92.3	94.8	93.2		knob	66.0	69.4	72.2	71.7
	leg	72.8	79.8	72.0	81.8	Pen	cap	51.0	30.3	54.6	25.9
	seat	90.1	95.0	89.1	91.1		button	48.0	48.5	52.4	52.1
	wheel	94.8	95.3	96.1	96.1	Phone	lid	28.8	28.1	16.5	23.0
Clock	hand	18.7	32.3	18.6	18.5		button	34.2	34.8	35.0	35.7
CoffeeMachine	button	1.3	1.3	1.3	1.4	Pliers	leg	3.2	4.1	31.1	31.1
	container	23.6	23.2	24.2	20.6	Printer	button	1.1	1.1	1.7	1.6
	knob	13.4	12.5	12.5	11.0	Refrigerator	door	27.2	25.6	20.4	19.6
	lid	24.8	24.9	24.0	22.3						
Dishwasher	door	49.0	49.0	48.8	53.5	Remote	button	19.9	20.3	29.6	33.7
	handle	31.7	34.4	40.6	47.1						
Dispenser	head	36.1	39.6	49.8	44.3	Safe	door	70.7	76.2	65.4	71.1
	lid	76.6	81.8	85.0	86.6		switch	19.3	19.3	20.2	21.8
Display	base	96.1	94.0	98.6	94.1		button	1.0	1.0	0.0	1.0
	screen	49.9	59.0	68.0	70.7	Scissors	blade	13.2	14.8	13.0	15.5
	support	60.9	52.0	45.6	51.9		handle	52.9	55.7	47.1	54.0
Door	frame	5.1	5.5	8.5	11.2		screw	4.8	6.0	9.2	9.9
	door	13.9	15.1	16.5	20.2	Stapler	body	86.1	86.6	87.0	87.0
	handle	23.9	23.8	27.7	28.1		lid	73.4	83.2	80.0	94.1
Eyeglasses	body	57.2	51.8	55.7	60.6	StorageFurniture	door	16.2	20.6	21.8	25.6
	leg	82.5	85.2	84.9	83.5		drawer	8.9	9.2	7.7	9.9
Faucet	spout	54.4	50.8	46.4	43.6		handle	62.1	71.5	58.7	71.1
	switch	31.5	28.9	30.5	27.0	Suitcase	handle	74.3	72.0	74.9	73.1
FoldingChair	seat	86.4	89.6	100.0	91.3		wheel	39.4	33.7	30.1	43.0
Globe	sphere	92.1	100.0	98.8	84.3	Switch	switch	21.2	22.2	19.7	22.1
Kettle	lid	67.7	88.9	88.9	82.0						
	handle	66.0	74.9	74.9	74.9	Table	door	0.0	0.0	0.0	0.0
	spout	68.6	68.6	57.3	66.3		drawer	8.9	10.9	11.6	10.1
Keyboard	cord	78.6	80.2	95.2	91.6		leg	40.2	42.4	40.4	40.4
		34.4	31.2	47.4	49.0		tabletop	61.4	63.1	67.7	68.3
KitchenPot	lid	95.1	95.1	69.8	76.4		wheel	73.0	54.3	61.9	66.6
	handle	39.9	53.8	49.6	57.4		handle	12.1	14.3	12.5	13.9
Knife	blade	44.5	41.3	39.2	32.3	Toaster	button	36.8	30.1	37.1	31.6
							slider	29.6	32.1	49.0	45.6
Lamp	base	84.4	81.5	71.6	76.5	Toilet	lid	49.7	54.9	47.5	57.2
	body	85.2	85.2	70.4	85.5		seat	2.1	6.1	1.4	5.0
	bulb	15.8	15.8	7.6	7.6		button	56.9	61.3	59.2	59.5
	shade	89.7	90.2	86.6	90.2	TrashCan	footpedal	0.0	0.0	0.0	0.0
Laptop	keyboard	54.5	67.6	62.4	70.1		lid	32.8	34.6	37.0	32.0
	screen	24.0	42.2	42.2	60.0	door	2.0	2.0	1.0	2.9	
	shaft	2.0	2.0	3.2	3.5	USB	cap	17.1	15.3	25.3	19.6
	touchpad	7.4	9.0	9.4	10.0		rotation	24.7	19.5	24.2	33.4
	camera	1.0	1.0	1.0	1.0	WashingMachine	door	35.3	27.4	35.6	22.9
Lighter	lid	38.9	38.9	17.2	29.8		button	12.4	12.4	17.3	17.3
	wheel	34.9	70.1	33.3	56.1	Window	window	23.6	19.3	26.1	20.0
	button	28.6	35.8	31.3	30.1						
Mean		41.6	44.7	44.2	45.6						

Table A4. Full table of part-aware instance segmentation results on the PartNet-Mobility [55] dataset.











































































































	Baselines		Ablations				Baselines		Ablations		
Category	SAM3D [62]	PartSLIP [32]	w/o Weight Pred.	w/o SAM Integration	Ours	Category	SAM3D [62]	PartSLIP [32]	w/o Weight Pred.	w/o SAM Integration	Ours
Bottle	15.3	73.4	74.9	79.5	76.2	Microwave	1.4	15.0	12.9	18.7	16.2
Box	18.2	56.3	72.2	60.7	69.6	Mouse	2.5	12.9	11.2	20.5	21.0
Bucket	12.0	10.2	78.2	39.3	78.2	Oven	1.0	46.8	55.6	56.4	62.0
Camera	2.2	37.1	35.5	37.8	37.0	Pen	8.2	40.8	35.8	47.2	34.5
Cart	8.5	69.5	74.0	68.3	71.2	Phone	1.1	31.0	33.3	31.6	34.7
Chair	5.7	80.7	81.1	81.2	83.3	Pliers	22.2	3.2	4.1	31.1	31.1
Clock	1.0	18.7	32.3	18.6	18.5	Printer	1.0	1.1	1.1	1.7	1.5
Coffee Machine	3.6	9.8	9.5	9.4	9.4	Refrigerator	1.8	27.7	30.5	19.4	22.0
Dishwasher	6.7	39.0	41.9	47.1	49.7	Remote	1.0	19.9	20.3	29.6	33.7
Dispenser	20.9	59.0	59.9	69.0	65.5	Safe	2.0	15.5	15.6	14.1	15.2
Display	34.1	61.5	66.4	66.0	68.4	Scissors	7.4	27.0	29.4	24.9	26.2
Door	17.2	11.5	11.6	13.9	16.0	Stapler	45.1	76.0	80.4	85.0	82.7
Eyeglasses	27.6	71.8	72.1	72.6	73.9	Storage Furniture	1.2	29.7	35.9	34.8	41.7
Faucet	23.7	42.8	37.1	37.9	35.6	Suitcase	1.8	47.3	46.2	47.1	43.8
FoldingChair	27.2	86.4	89.6	100.0	91.3	Switch	5.0	21.2	22.2	19.7	22.4
Globe	4.2	92.1	100.0	98.8	84.3	Table	10.8	28.7	29.2	27.6	28.2
Kettle	41.8	69.5	75.3	76.3	75.9	Toaster	1.8	34.8	35.9	38.6	39.2
Keyboard	1.0	34.1	31.0	47.3	48.9	Toilet	3.6	35.4	40.0	36.6	41.0
KitchenPot	31.9	55.4	66.2	52.3	65.4	TrashCan	7.6	22.6	24.5	24.3	22.8
Knife	2.2	44.5	41.3	39.2	32.1	USB	23.4	20.5	15.2	27.3	23.5
Lamp	48.4	77.0	77.7	66.5	75.9	Washing Machine	2.8	17.5	14.6	21.4	19.6
Laptop	1.9	19.5	26.5	27.4	34.1	Window	18.0	23.6	19.3	26.1	19.5
Lighter	8.9	32.7	49.9	26.6	39.8	Mean	12.1	38.9	42.6	42.6	44.1



























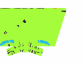





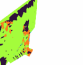





















































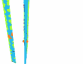


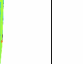


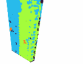























































































Table A5. Full table of part-agnostic instance segmentation results on the PartNet-Mobility [55] dataset.

A.5. Additional Qualitative Results for Semantic Segmentation














































































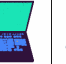
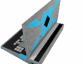


























































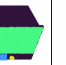








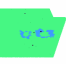



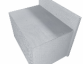

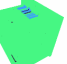



























We present additional part segmentation results below, encompassing semantic segmentation. Each row shows the same object with different views.

view 1						view 2					
Input	GT	SATR [2]	SATR [2]+SPPartSLIP [32]	PARTSTAD (Ours)		Input	GT	SATR [2]	SATR [2]+SPPartSLIP [32]	PARTSTAD (Ours)	

view 1						view 2					
Input	GT	SATR [2]	SATR [2]+SPPartSLIP [32]	PARTSTAD (Ours)		Input	GT	SATR [2]	SATR [2]+SPPartSLIP [32]	PARTSTAD (Ours)	
											
											
											
											
											
											
											
											
											
											
											
											
											
											
											

view 1						view 2					
Input	GT	SATR [2]	SATR [2]+SPPartSLIP [32]	PARTSTAD (Ours)		Input	GT	SATR [2]	SATR [2]+SPPartSLIP [32]	PARTSTAD (Ours)	
											
											
											
											
											
											
											
											
											
											
											
											
											
											
											

view 1						view 2					
Input	GT	SATR [2]	SATR [2]+SP	PartSLIP [32]	PARTSTAD (Ours)	Input	GT	SATR [2]	SATR [2]+SP	PartSLIP [32]	PARTSTAD (Ours)


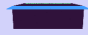

























































































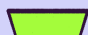






































view 1						view 2					
Input	GT	SATR [2]	SATR [2]+SPPartSLIP [32]	PARTSTAD (Ours)		Input	GT	SATR [2]	SATR [2]+SPPartSLIP [32]	PARTSTAD (Ours)	
											
											
											
											
											
											
											
											
											
											
											
											
											
											
											

view 1						view 2					
Input	GT	SATR [2]	SATR [2]+SP	PartSLIP [32]	PARTSTAD (Ours)	Input	GT	SATR [2]	SATR [2]+SP	PartSLIP [32]	PARTSTAD (Ours)

































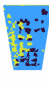

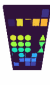































































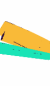








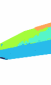





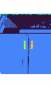














































view 1						view 2					
Input	GT	SATR [2]	SATR [2]+SPPartSLIP [32]	PARTSTAD (Ours)		Input	GT	SATR [2]	SATR [2]+SPPartSLIP [32]	PARTSTAD (Ours)	


















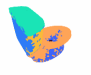












A.6. Additional Qualitative Results for Instance Segmentation

We present additional part segmentation results below, encompassing instance segmentation. Each row shows the same object with different views.

view 1					view 2				
Input	GT	SAM3D [62]	PartSLIP [32]	PARTSTAD (Ours)	Input	GT	SAM3D [62]	PartSLIP [32]	PARTSTAD (Ours)
									
									
									
									
									
									
									
									
									
									
									
									
									

view 1					view 2				
Input	GT	SAM3D [62]	PartSLIP [32]	PARTSTAD (Ours)	Input	GT	SAM3D [62]	PartSLIP [32]	PARTSTAD (Ours)

view 1					view 2				
Input	GT	SAM3D [62]	PartSLIP [32]	PARTSTAD (Ours)	Input	GT	SAM3D [62]	PartSLIP [32]	PARTSTAD (Ours)
									
									
									
									
									
									
									
									
									
									
									
									
									
									
									
									

view 1					view 2				
Input	GT	SAM3D [62]	PartSLIP [32]	PARTSTAD (Ours)	Input	GT	SAM3D [62]	PartSLIP [32]	PARTSTAD (Ours)
									
									
									

References

- [1] Ahmed Abdelreheem, Abdelrahman Eldesokey, Maks Ovsjanikov, and Peter Wonka. Zero-shot 3D shape correspondence. In *SIGGRAPH Asia*, 2023. 3
- [2] Ahmed Abdelreheem, Ivan Skorokhodov, Maks Ovsjanikov, and Peter Wonka. SATR: Zero-shot semantic segmentation of 3D shapes. In *ICCV*, 2023. 1, 3, 6, 7, 12, 15, 16, 17, 18, 19, 20, 21
- [3] Iro Armeni, Sasha Sax, Amir R Zamir, and Silvio Savarese. Joint 2D-3D-semantic data for indoor scene understanding. *arXiv preprint arXiv:1702.01105*, 2017. 2
- [4] Dmitry Baranchuk, Andrey Voynov, Ivan Rubachev, Valentin Khrulkov, and Artem Babenko. Label-efficient semantic segmentation with diffusion models. In *ICLR*, 2022. 3
- [5] J. Behley, M. Garbade, A. Milioto, J. Quenzel, S. Behnke, C. Stachniss, and J. Gall. SemanticKITTI: A dataset for semantic scene understanding of LiDAR sequences. In *ICCV*, 2019. 2
- [6] Jiazhong Cen, Zanwei Zhou, Jiemin Fang, Chen Yang, Wei Shen, Lingxi Xie, Xiaopeng Zhang, and Qi Tian. Segment anything in 3D with nerfs. In *NeurIPS*, 2023. 3
- [7] Angel Chang, Angela Dai, Thomas Funkhouser, Maciej Halber, Matthias Niessner, Manolis Savva, Shuran Song, Andy Zeng, and Yinda Zhang. Matterport3D: Learning from rgb-d data in indoor environments. In *3DV*, 2017. 2
- [8] Angel X Chang, Thomas Funkhouser, Leonidas Guibas, Pat Hanrahan, Qixing Huang, Zimo Li, Silvio Savarese, Manolis Savva, Shuran Song, Hao Su, et al. ShapeNet: An information-rich 3D model repository. *arXiv preprint arXiv:1512.03012*, 2015. 2
- [9] Runnan Chen, Youquan Liu, Lingdong Kong, Xinge Zhu, Yuexin Ma, Yikang Li, Yuenan Hou, Yu Qiao, and Wenping Wang. CLIP2Scene: Towards label-efficient 3D scene understanding by clip. In *CVPR*, 2023. 2
- [10] Julian Chibane, Francis Engelmann, Tuan Anh Tran, and Gerard Pons-Moll. Box2Mask: Weakly supervised 3D semantic instance segmentation using bounding boxes. In *ECCV*, 2022. 2
- [11] Ruihang Chu, Yukang Chen, Tao Kong, Lu Qi, and Lei Li. ICM-3D: Instantiated category modeling for 3d instance segmentation. *IEEE Robotics and Automation Letters*, 2021. 2
- [12] Angela Dai, Angel X. Chang, Manolis Savva, Maciej Halber, Thomas Funkhouser, and Matthias Nießner. ScanNet: Richly-annotated 3D reconstructions of indoor scenes. In *CVPR*, 2017. 2
- [13] Dale DeCatur, Itai Lang, and Rana Hanocka. 3D Highlighter: Localizing regions on 3D shapes via text descriptions. In *CVPR*, 2023. 2, 3
- [14] Timo Hackel, N. Savinov, L. Ladicky, Jan D. Wegner, K. Schindler, and M. Pollefeys. SEMANTIC3D.NET: A new large-scale point cloud classification benchmark. In *ISPRS Annals of the Photogrammetry, Remote Sensing and Spatial Information Sciences*, 2017. 2
- [15] Ji Hou, Angela Dai, and Matthias Nießner. 3D-SIS: 3D semantic instance segmentation of rgb-d scans. In *CVPR*, 2019. 2
- [16] Edward J Hu, Yelong Shen, Phillip Wallis, Zeyuan Allen-Zhu, Yuanzhi Li, Shean Wang, Lu Wang, and Weizhu Chen. LoRA: Low-rank adaptation of large language models. *arXiv preprint arXiv:2106.09685*, 2021. 2, 5
- [17] Rongzhou Huang, Chuyin Huang, Yubao Liu, Genan Dai, and Weiyang Kong. LSGCN: Long short-term traffic prediction with graph convolutional networks. In *IJCAI*, 2020. 2
- [18] Zhening Huang, Xiaoyang Wu, Xi Chen, Hengshuang Zhao, Lei Zhu, and Joan Lasenby. OpenIns3D: Snap and lookup for 3D open-vocabulary instance segmentation. *arXiv preprint*, 2023. 3
- [19] Li Jiang, Hengshuang Zhao, Shaoshuai Shi, Shu Liu, Chi-Wing Fu, and Jiaya Jia. PointGroup: Dual-set point grouping for 3D instance segmentation. In *CVPR*, 2020. 2
- [20] Alexander Kirillov, Eric Mintun, Nikhila Ravi, Hanzi Mao, Chloe Rolland, Laura Gustafson, Tete Xiao, Spencer Whitehead, Alexander C Berg, Wan-Yen Lo, et al. Segment anything. *arXiv preprint arXiv:2304.02643*, 2023. 1, 2, 3, 4, 5, 6, 9
- [21] Juil Koo, Ian Huang, Panos Achlioptas, Leonidas J Guibas, and Minhyuk Sung. PartGlott: Learning shape part segmentation from language reference games. In *CVPR*, 2022. 2
- [22] Xin Lai, Zhuotao Tian, Yukang Chen, Yanwei Li, Yuhui Yuan, Shu Liu, and Jiaya Jia. LISA: Reasoning segmentation via large language model. *arXiv preprint arXiv:2308.00692*, 2023. 3
- [23] Eric-Tuan Lê, Minhyuk Sung, Duygu Ceylan, Radomir Mech, Tamy Boubekeur, and Niloy J. Mitra. CPFN: Cascaded primitive fitting networks for high-resolution point clouds. In *ICCV*, 2021. 2
- [24] Lingxiao Li, Minhyuk Sung, Anastasia Dubrovina, Li Yi, and Leonidas J Guibas. Supervised fitting of geometric primitives to 3D point clouds. In *CVPR*, 2019. 2, 4
- [25] Liunian Harold Li, Pengchuan Zhang, Haotian Zhang, Jianwei Yang, Chunyuan Li, Yiwu Zhong, Lijuan Wang, Lu Yuan, Lei Zhang, Jenq-Neng Hwang, et al. Grounded language-image pre-training. In *CVPR*, 2022. 1, 2, 3, 5, 6, 9
- [26] Mengtian Li, Yuan Xie, Yunhang Shen, Bo Ke, Ruizhi Qiao, Bo Ren, Shaohui Lin, and Lizhuang Ma. Hybridcr: Weakly-supervised 3d point cloud semantic segmentation via hybrid contrastive regularization. In *CVPR*, 2022. 2
- [27] Yangyan Li, Rui Bu, Mingchao Sun, Wei Wu, Xinhan Di, and Baoquan Chen. PointCNN: Convolution on x-transformed points. In *NeurIPS*, 2018. 2
- [28] Ying Li, Lingfei Ma, Zilong Zhong, Dongpu Cao, and Jonathan Li. TGNet: Geometric graph cnn on 3D point cloud segmentation. *IEEE Transactions on Geoscience and Remote Sensing*, 2019. 2
- [29] Zhidong Liang, Ming Yang, Hao Li, and Chunxiang Wang. 3D instance embedding learning with a structure-aware loss function for point cloud segmentation. *IEEE Robotics and Automation Letters*, 2020. 2
- [30] Tsung-Yi Lin, Michael Maire, Serge Belongie, James Hays, Pietro Perona, Deva Ramanan, Piotr Dollár, and C Lawrence Zitnick. Microsoft COCO: Common objects in context. In *ECCV*, 2014. 1

- [31] Jinxian Liu, Minghui Yu, Bingbing Ni, and Ye Chen. Self-prediction for joint instance and semantic segmentation of point clouds. In *ECCV*, 2020. 2
- [32] Minghua Liu, Yinhao Zhu, Hong Cai, Shizhong Han, Zhan Ling, Fatih Porikli, and Hao Su. PartSLIP: Low-shot part segmentation for 3d point clouds via pretrained image-language models. In *CVPR*, 2023. 1, 2, 3, 5, 6, 7, 8, 9, 11, 12, 13, 14, 15, 16, 17, 18, 19, 20, 21, 22, 23, 24, 25
- [33] Shilong Liu, Zhaoyang Zeng, Tianhe Ren, Feng Li, Hao Zhang, Jie Yang, Chunyuan Li, Jianwei Yang, Hang Su, Jun Zhu, et al. Grounding DINO: Marrying dino with grounded pre-training for open-set object detection. *arXiv preprint arXiv:2303.05499*, 2023. 3
- [34] Yongcheng Liu, Bin Fan, Gaofeng Meng, Jiwen Lu, Shiming Xiang, and Chunhong Pan. DensePoint: Learning densely contextual representation for efficient point cloud processing. In *ICCV*, 2019. 2
- [35] Zhengzhe Liu, Xiaojuan Qi, and Chi-Wing Fu. One thing one click: A self-training approach for weakly supervised 3D semantic segmentation. In *CVPR*, 2021. 2
- [36] Xu Ma, Can Qin, Haoxuan You, Haoxi Ran, and Yun Fu. Rethinking network design and local geometry in point cloud: A simple residual mlp framework. In *ICLR*, 2022. 2
- [37] Kaichun Mo, Shilin Zhu, Angel X. Chang, Li Yi, Subarna Tripathi, Leonidas J. Guibas, and Hao Su. PartNet: A large-scale benchmark for fine-grained and hierarchical part-level 3D object understanding. In *CVPR*, 2019. 1, 2
- [38] Gaku Narita, Takashi Seno, Tomoya Ishikawa, and Yohsuke Kaji. Panopticfusion: Online volumetric semantic mapping at the level of stuff and things. In *IROS*, 2019. 2
- [39] Songyou Peng, Kyle Genova, Chiyu Jiang, Andrea Tagliasacchi, Marc Pollefeys, Thomas Funkhouser, et al. OpenScene: 3D scene understanding with open vocabularies. In *CVPR*, 2023. 2
- [40] Quang-Hieu Pham, Duc Thanh Nguyen, Binh-Son Hua, Gemma Roig, and Sai-Kit Yeung. JSIS3D: Joint semantic-instance segmentation of 3D point clouds with multi-task pointwise networks and multi-value conditional random fields. In *CVPR*, 2019. 2
- [41] Yada Pruksachatkun, Jason Phang, Haokun Liu, Phu Mon Htut, Xiaoyi Zhang, Richard Yuanzhe Pang, Clara Vania, Katharina Kann, and Samuel R. Bowman. Intermediate-Task Transfer Learning with Pretrained Language Models: When and why does it work? In *ACL*, 2020. 3
- [42] Charles R Qi, Hao Su, Kaichun Mo, and Leonidas J Guibas. PointNet: Deep learning on point sets for 3d classification and segmentation. In *CVPR*, 2017. 2
- [43] Charles Ruizhongtai Qi, Li Yi, Hao Su, and Leonidas J Guibas. PointNet++: Deep hierarchical feature learning on point sets in a metric space. In *NeurIPS*, 2017. 2
- [44] Guocheng Qian, Yuchen Li, Houwen Peng, Jinjie Mai, Hasan Hammoud, Mohamed Elhoseiny, and Bernard Ghanem. PointNext: Revisiting pointnet++ with improved training and scaling strategies. In *NeurIPS*, 2022. 2
- [45] Alec Radford, Jong Wook Kim, Chris Hallacy, Aditya Ramesh, Gabriel Goh, Sandhini Agarwal, Girish Sastry, Amanda Askell, Pamela Mishkin, Jack Clark, et al. Learning transferable visual models from natural language supervision. In *ICML*, 2021. 2, 3
- [46] Jonas Schult, Francis Engelmann, Alexander Hermans, Or Litany, Siyu Tang, and Bastian Leibe. Mask3D: Mask transformer for 3D semantic instance segmentation. In *ICRA*, 2023. 2
- [47] Ayça Takmaz, Elisabetta Fedele, Robert W. Sumner, Marc Pollefeys, Federico Tombari, and Francis Engelmann. OpenMask3D: Open-vocabulary 3D instance segmentation. In *NeurIPS*, 2023. 2, 3
- [48] Luming Tang, Menglin Jia, Qianqian Wang, Cheng Phoo, and Bharath Hariharan. Emergent correspondence from image diffusion. In *NeurIPS*, 2023. 3
- [49] Hugues Thomas, Charles R Qi, Jean-Emmanuel Deschaud, Beatriz Marcotegui, François Goulette, and Leonidas J Guibas. Kpconv: Flexible and deformable convolution for point clouds. In *ICCV*, 2019. 2
- [50] Thang Vu, Kookhoi Kim, Tung M. Luu, Xuan Thanh Nguyen, and Chang D. Yoo. Softgroup for 3d instance segmentation on 3D point clouds. In *CVPR*, 2022. 2
- [51] Weiyue Wang, Ronald Yu, Qiangui Huang, and Ulrich Neumann. SGPn: Similarity group proposal network for 3D point cloud instance segmentation. In *CVPR*, 2018. 2
- [52] Xinlong Wang, Shu Liu, Xiaoyong Shen, Chunhua Shen, and Jiaya Jia. Associatively segmenting instances and semantics in point clouds. In *CVPR*, 2019. 2
- [53] Yue Wang, Yongbin Sun, Ziwei Liu, Sanjay E. Sarma, Michael M. Bronstein, and Justin M. Solomon. Dynamic graph cnn for learning on point clouds. *ACM TOG*, 2019. 2
- [54] Xiaoyang Wu, Yixing Lao, Li Jiang, Xihui Liu, and Hengshuang Zhao. Point transformer v2: Grouped vector attention and partition-based pooling. In *NeurIPS*, 2022. 2
- [55] Fanbo Xiang, Yuzhe Qin, Kaichun Mo, Yikuan Xia, Hao Zhu, Fangchen Liu, Minghua Liu, Hanxiao Jiang, Yifu Yuan, He Wang, Li Yi, Angel X. Chang, Leonidas J. Guibas, and Hao Su. SAPIEN: A simulated part-based interactive environment. In *CVPR*, 2020. 2, 6, 12, 13, 14
- [56] Tiange Xiang, Chaoyi Zhang, Yang Song, Jianhui Yu, and Weidong Cai. Walk in the Cloud: Learning curves for point clouds shape analysis. In *ICCV*, 2021. 2
- [57] Jiarui Xu, Sifei Liu, Arash Vahdat, Wonmin Byeon, Xiaolong Wang, and Shalini De Mello. Open-vocabulary panoptic segmentation with text-to-image diffusion models. In *CVPR*, 2023. 3
- [58] Mutian Xu, Runyu Ding, Hengshuang Zhao, and Xiaojuan Qi. PACnv: Position adaptive convolution with dynamic kernel assembling on point clouds. In *CVPR*, 2021. 2
- [59] Xu Yan, Chaoda Zheng, Zhen Li, Sheng Wang, and Shuguang Cui. PointANSL: Robust point clouds processing using nonlocal neural networks with adaptive sampling. In *CVPR*, 2020. 2
- [60] Bo Yang, Jianan Wang, Ronald Clark, Qingyong Hu, Sen Wang, Andrew Markham, and Niki Trigoni. Learning object bounding boxes for 3D instance segmentation on point clouds. In *NeurIPS*, 2019. 2
- [61] Xingyi Yang and Xinchao Wang. Diffusion model as representation learner. In *ICCV*, 2023. 3

- [62] Yunhan Yang, Xiaoyang Wu, Tong He, Hengshuang Zhao, and Xihui Liu. SAM3D: Segment anything in 3D scenes. *arXiv preprint arXiv:2306.03908*, 2023. 3, 6, 7, 8, 14, 22, 23, 24, 25
- [63] Kwang Moo Yi, Eduard Trulls, Yuki Ono, Vincent Lepetit, Mathieu Salzmann, and Pascal Fua. Learning to find good correspondences. In *CVPR*, 2018. 5
- [64] Li Yi, Haibin Huang, Difan Liu, Evangelos Kalogerakis, Hao Su, and Leonidas Guibas. Deep part induction from articulated object pairs. *ACM TOG*, 2018. 4
- [65] Li Yi, Wang Zhao, He Wang, Minhyuk Sung, and Leonidas J Guibas. GSPN: Generative shape proposal network for 3D instance segmentation in point cloud. In *CVPR*, 2019. 2
- [66] Xumin Yu, Lulu Tang, Yongming Rao, Tiejun Huang, Jie Zhou, and Jiwen Lu. Point-BERT: Pre-training 3D point cloud transformers with masked point modeling. In *CVPR*, 2022. 2
- [67] Amir R. Zamir, Alexander Sax, William B. Shen, Leonidas J. Guibas, Jitendra Malik, and Silvio Savarese. Taskonomy: Disentangling task transfer learning. In *CVPR*, 2018. 3
- [68] Biao Zhang and Peter Wonka. Point cloud instance segmentation using probabilistic embeddings. In *CVPR*, 2021. 2
- [69] Junbo Zhang, Runpei Dong, and Kaisheng Ma. CLIP-FO3D: Learning free open-world 3D scene representations from 2D dense clip. *arXiv preprint arXiv:2303.04748*, 2023. 2
- [70] Renrui Zhang, Liuhui Wang, Yali Wang, Peng Gao, Hongsheng Li, and Jianbo Shi. Parameter is not all you need: Starting from non-parametric networks for 3D point cloud analysis. In *CVPR*, 2023. 2
- [71] Yuxuan Zhang, Huan Ling, Jun Gao, Kangxue Yin, Jean-Francois Lafleche, Adela Barriuso, Antonio Torralba, and Sanja Fidler. DatasetGAN: Efficient labeled data factory with minimal human effort. In *CVPR*, 2021. 3
- [72] Hengshuang Zhao, Li Jiang, Jiaya Jia, Philip HS Torr, and Vladlen Koltun. Point transformer. In *ICCV*, 2021. 2
- [73] Na Zhao, Tat-Seng Chua, and Gim Hee Lee. Few-shot 3D point cloud semantic segmentation. In *CVPR*, 2021. 2